(Received 21 April 2025, Accepted 6 June 2025, Scheduled 6 July 2025)

Tuned Y-Shaped Electromagnetic Switch for Directional Signal Control in Photonic Circuits

Imane Chaker[1,*], Ilham El-Atmani[1], Fatima-Zahra Berahioui[1], Younes Errouas[1,2], Amina Ghadban[1], Farid Falyouni[1], Khalid Laabidi[1], Driss Bria[1], and Yan Pennec[3]

[1]*Laboratory of Materials, Waves, Energy and Environment, Team of Waves, Acoustic, Photonic and Materials Faculty of Sciences, Mohammed First University, Oujda, Morocco*
[2]*Laboratory of Sciences and Techniques for Engineering (LaSTI), National School of Applied Sciences Khouribga Sultan Moulay Slimane University (USMS), Beni Mellal, Morocco*
[3]*Institut d'Electronique, de Microélectronique et de Nanotechnologie (IEMN), UMR CNRS 8520 Université de Lille, 59650 Villeneuve d'Ascq, France*

ABSTRACT: In this study, we present a Y-shaped electromagnetic waveguide switch with integrated resonators designed to control wave propagation within a specific frequency range. The switch comprises two input lines and one output line, with each input line connected to a resonator of height d_1 and d_3 that can either allow or block transmission of the signal. Using the Transfer Matrix Method (TMM), we determined transmission and reflection properties to analyze the device's performance in ON (transmission) and OFF (blocking) states. Our results indicate that, depending on the choice of geometric and structural parameters, the resonators enable a transmission of more than 99% (T_{13}) from the first input line to the output line in the ON state, while reducing the transmission from the second input line to less than 1% (T_{23}) in the OFF state. These findings show the importance of resonator tuning for achieving precise electromagnetic wave control, offering a practical approach for enhancing signal management in advanced optical communication systems.

1. INTRODUCTION

Electromagnetic waveguide switches are critical components in advanced signal processing and telecommunication systems, enabling dynamic control over the propagation of electromagnetic waves by adjusting signal direction and intensity within confined structures [1–6]. These switches are integral to modern optical communication networks and integrated photonic circuits, where they significantly improve sensing capabilities [7–10]. Their versatility and performance have been frequently in extensive use in data centers for high-speed data routing, in reconfigurable antennas to achieve flexible signal direction control and in optical computing platforms to support rapid signal processing and related operations [11, 12]. Such general uses improve the importance of electromagnetic waveguide switches in high-performance communication and processing environments.

In addition to their contributions to communication networks, electromagnetic waveguide switches are essential for imaging and environmental sensing applications. By precisely manipulating electromagnetic fields, these switches have the potential to enhance image clarity, facilitate detailed environmental analysis, and allow the detection of signal variations critical for both research and monitoring [4, 13–16]. Thus, there has been a great deal of research into new switch designs that ensure high efficiency, solid performance, flexibility, and simple integration with current platforms in response to growing demands for faster, more flexible communication systems.

Numerous approaches have been explored to satisfy these changing requirements. For example, Dao et al. [17] presented a compact 2×2 photonic switch consisting of a waveguide with a phase-change material (Sb_2Se_3) for switching. This system efficiently connects two inputs to two outputs, facilitating low-loss signal routing. Rehman et al. [18] introduced a three-dimensional switch based on guided mode resonances in photonic crystals, achieving a significant 13.75% data signal enhancement at a wavelength of 1.55 µm. Similarly, Rehman et al. [19] employed crystal cavity methods to improve switching efficiency by approximately 7%. In addition, Hu et al. [1] exploited Fano resonance phenomena to realize high modulation intensity terahertz switches, making the way for future high speed communication systems.

In this study, we investigate a Y-shaped electromagnetic waveguide switch composed of two input channels and one output channel, integrating resonators to ensure precise directional control of electromagnetic waves to achieve the switch phenomenon. Using transfer matrix method (TMM), we calculate transmission and reflection rates, enabling a thorough analysis of the switch's ON and OFF states. Subsequently, we examine the influence of resonator parameters on switching performance and identify optimal configurations for distinct transmission states. We conclude by summarizing our main findings and discussing their potential applications in optical communication and photonics.

* Corresponding author: Imane Chaker (imane.chaker@ump.ac.ma).

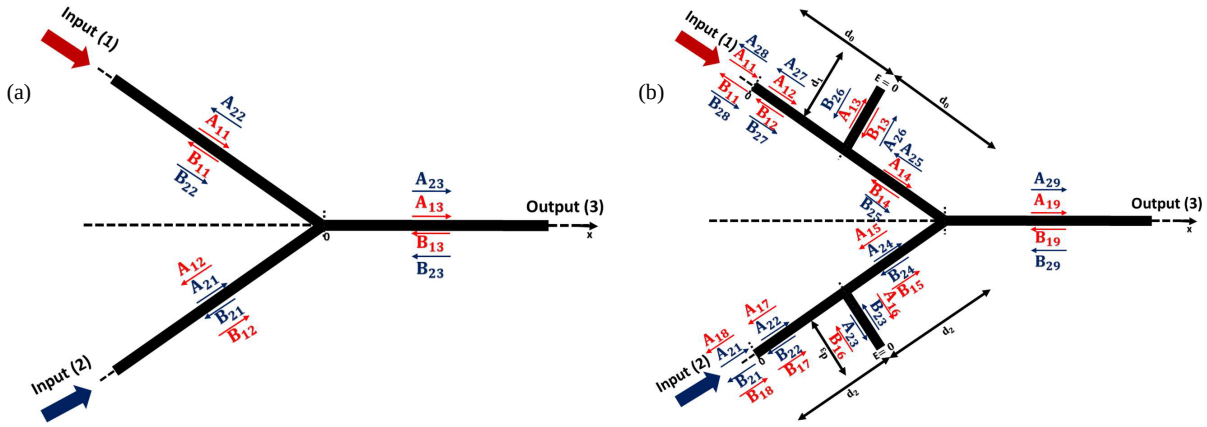

FIGURE 1. (a) Y-shaped electromagnetic switch without resonator. (b) Y-shaped electromagnetic switch with two resonators of height d_1 and d_3 grafted into the first and second input lines respectively.

2. THEORETICAL FORMALISM

The transfer matrix method (TMM) is commonly used to study waveguides and to analyze properties such as reflection and transmission rates. This approach considers the evolution of the electromagnetic field as it passes through different sections of the waveguide, while ensuring consistency with the boundary conditions at each interface. This method is particularly useful for electromagnetic waveguide systems and can be used in a variety of fields, such as electronics and acoustics [20–26].

In Fig. 1(a), we examine a structure composed of two inputs and one output channels composed of waveguides. In Fig. 1(b), we illustrate a structure comprising two input channels and one output line. The first input includes two segments of lengths d_0, connected by a resonator of height d_1. The second input consists of two segments of lengths d_2, grafted at their middle by one resonator of height d_3. In this study, we use Transfer Matrix Method (TMM) to analyze electromagnetic wave propagation in a one-dimensional waveguide system Y-shaped electromagnetic switch (Fig. 1).

2.1. Analysis of Transmission and Reflection Rates in an Electromagnetic Switch without Resonator

In this section, we calculate the transfer matrix for a Y-shaped system electromagnetic switch without resonator (Fig. 1(a)). The expressions for the electric fields in the three regions of the system are as follows:

$$E(x)=\begin{cases} E_{11}(x)=A_{11}e^{j\alpha_0 x}+B_{11}e^{-j\alpha_0 x} & \text{for}: x\le 0\\ E_{12}(x)=A_{12}e^{j\alpha_1 x}+B_{12}e^{-j\alpha_1 x} & \text{for}: x\le 0\\ E_{13}(x)=A_{13}e^{j\alpha_2 x}+B_{13}e^{-j\alpha_2 x} & \text{for}: x\ge 0\\ E_{21}(x)=A_{21}e^{j\alpha_1 x}+B_{21}e^{-j\alpha_1 x} & \text{for}: x\le 0\\ E_{22}(x)=A_{22}e^{j\alpha_0 x}+B_{22}e^{-j\alpha_0 x} & \text{for}: x\le 0\\ E_{23}(x)=A_{23}e^{j\alpha_2 x}+B_{23}e^{-j\alpha_2 x} & \text{for}: x\ge 0 \end{cases} \quad (1)$$

The electric field within each medium is expressed as the sum of an incident wave and a reflected wave. The amplitudes A_{1i}, B_{1i}, A_{2i}, B_{2i} (for $i = [1\text{–}3]$) represent the amplitudes of the progressive and regressive electromagnetic waves.

We define $\alpha_i = \frac{\omega}{c}\sqrt{\varepsilon_i \mu_i}$, for $i = [0, 2]$ where ω is the angular frequency of the incoming electromagnetic wave, ε_i the relative permittivity, μ_i the permeability of the non-magnetic medium, and c the speed of electromagnetic waves in a vacuum.

The conditions of passage in $x = 0$ are:

$$\begin{cases} E_{11}(x=0)=E_{12}(x=0)=E_{13}(x=0)\\ \frac{dE_{11}}{dx}\big)_{x=0}=\frac{dE_{12}}{dx}\big)_{x=0}+\frac{dE_{13}}{dx}\big)_{x=0}\\ E_{21}(x=0)=E_{22}(x=0)=E_{23}(x=0)\\ \frac{dE_{21}}{dx}\big)_{x=0}=\frac{dE_{22}}{dx}\big)_{x=0}+\frac{dE_{23}}{dx}\big)_{x=0} \end{cases} \quad (2)$$

By applying the calculations described in system (2), we obtain the following results:

$$\begin{pmatrix} A_{11}\\ B_{11}\end{pmatrix}=\begin{pmatrix} \frac{\alpha_0+\alpha_1}{2\alpha_0} & \frac{\alpha_0-\alpha_1}{2\alpha_0} & \frac{\alpha_2}{2\alpha_0} & \frac{-\alpha_2}{2\alpha_0}\\ \frac{\alpha_0-\alpha_1}{2\alpha_0} & \frac{\alpha_0+\alpha_1}{2\alpha_0} & \frac{-\alpha_2}{2\alpha_0} & \frac{\alpha_2}{2\alpha_0}\end{pmatrix}\begin{pmatrix} A_{12}\\ B_{12}\\ A_{13}\\ B_{13}\end{pmatrix} \quad (3)$$

The matrix: $T_1=\begin{pmatrix} \frac{\alpha_0+\alpha_1}{2\alpha_0} & \frac{\alpha_0-\alpha_1}{2\alpha_0} & \frac{\alpha_2}{2\alpha_0} & \frac{-\alpha_2}{2\alpha_0}\\ \frac{\alpha_0-\alpha_1}{2\alpha_0} & \frac{\alpha_0+\alpha_1}{2\alpha_0} & \frac{-\alpha_2}{2\alpha_0} & \frac{\alpha_2}{2\alpha_0}\end{pmatrix}$ defines the connections between the input amplitudes A_{11} and B_{11} from the first input line and the output amplitudes A_{12}, B_{12}, A_{13} and B_{13} within our electromagnetic switching system.

To simplify, we represent the matrix T_1 using a notation:

$$T_1=\begin{pmatrix} Y_{11} & Y_{12} & Y_{13} & Y_{14}\\ Y_{15} & Y_{16} & Y_{17} & Y_{18}\end{pmatrix} \quad (4)$$

Then,

$$\begin{pmatrix} A_{21}\\ B_{21}\end{pmatrix}=\begin{pmatrix} \frac{\alpha_1+\alpha_0}{2\alpha_1} & \frac{\alpha_1-\alpha_0}{2\alpha_1} & \frac{\alpha_2}{2\alpha_1} & \frac{-\alpha_2}{2\alpha_1}\\ \frac{\alpha_1-\alpha_0}{2\alpha_1} & \frac{\alpha_1+\alpha_0}{2\alpha_1} & \frac{-\alpha_2}{2\alpha_1} & \frac{\alpha_2}{2\alpha_1}\end{pmatrix}\begin{pmatrix} A_{22}\\ B_{22}\\ A_{23}\\ B_{23}\end{pmatrix} \quad (5)$$

The matrix : $T_2=\begin{pmatrix} \frac{\alpha_1+\alpha_0}{2\alpha_1} & \frac{\alpha_1-\alpha_0}{2\alpha_1} & \frac{\alpha_2}{2\alpha_1} & \frac{-\alpha_2}{2\alpha_1}\\ \frac{\alpha_1-\alpha_0}{2\alpha_1} & \frac{\alpha_1+\alpha_0}{2\alpha_1} & \frac{-\alpha_2}{2\alpha_1} & \frac{\alpha_2}{2\alpha_1}\end{pmatrix}$ defines

the connections between the input amplitudes A_{21} and B_{21} the second input line and the output amplitudes A_{22}, B_{22}, A_{23} and B_{23} within our electromagnetic switching system.

To simplify, we represent the matrix T_2 using a notation:

$$T_2 = \begin{pmatrix} Y_{21} & Y_{22} & Y_{23} & Y_{24} \\ Y_{25} & Y_{26} & Y_{27} & Y_{28} \end{pmatrix} \tag{6}$$

Using formulations (3) and (5), we obtain the following form of the global matrix for our proposed system without resonator:

$$\begin{pmatrix} A_{11} \\ B_{11} \\ A_{21} \\ B_{21} \end{pmatrix} = T_{S_1} \begin{pmatrix} A_{12} \\ B_{12} \\ A_{13} \\ B_{13} \\ A_{22} \\ B_{22} \\ A_{23} \\ B_{23} \end{pmatrix} \tag{7}$$

With $T_{S_1} = \begin{pmatrix} a_{11} & a_{12} & a_{13} & a_{14} & a_{15} & a_{16} & a_{17} & a_{18} \\ a_{21} & a_{22} & a_{23} & a_{24} & a_{25} & a_{26} & a_{27} & a_{28} \\ a_{31} & a_{32} & a_{33} & a_{34} & a_{35} & a_{36} & a_{37} & a_{38} \\ a_{41} & a_{42} & a_{43} & a_{44} & a_{45} & a_{46} & a_{47} & a_{48} \end{pmatrix}$.

The transmission and reflection coefficients are represented by the following formulas:

$$\begin{cases} t_{12} = \frac{A_{12}}{A_{11}}\Big)_{\substack{B_{12}=0 \\ B_{13}=0 \\ B_{21}=0 \\ B_{23}=0}} = \frac{1}{a_{11}+a_{13}} \\ t_{13} = \frac{A_{13}}{A_{11}}\Big)_{\substack{B_{12}=0 \\ B_{13}=0 \\ B_{21}=0 \\ B_{23}=0}} = \frac{1}{a_{11}+a_{13}} \\ r_{11} = \frac{B_{11}}{A_{11}}\Big)_{\substack{B_{12}=0 \\ B_{13}=0 \\ B_{21}=0 \\ B_{23}=0}} = \frac{a_{21}+a_{23}}{a_{11}+a_{13}} \\ t_{21} = \frac{A_{22}}{A_{21}}\Big)_{\substack{B_{12}=0 \\ B_{13}=0 \\ B_{21}=0 \\ B_{23}=0}} = \frac{1}{a_{35}+a_{37}} \\ t_{23} = \frac{A_{23}}{A_{21}}\Big)_{\substack{B_{12}=0 \\ B_{13}=0 \\ B_{21}=0 \\ B_{23}=0}} = \frac{1}{a_{35}+a_{37}} \\ r_{22} = \frac{B_{21}}{A_{21}}\Big)_{\substack{B_{12}=0 \\ B_{13}=0 \\ B_{21}=0 \\ B_{23}=0}} = \frac{a_{45}+a_{47}}{a_{35}+a_{37}} \end{cases} \tag{8}$$

where:

- t_{12}: transmission from input channel 1 through input channel 2.
- t_{13}: transmission from input channel 1 through output channel.
- r_{11}: reflection from input channel 1.
- t_{21}: transmission from input channel 2 through input channel 1.
- t_{23}: transmission from input channel 2 through output channel.
- r_{22}: reflection from input channel 2.

The transmission and reflection rates are expressed as follows:

$$\begin{cases} T_{12} = |t_{12}|^2 = \left|\frac{1}{a_{11}+a_{13}}\right|^2 \\ T_{13} = |t_{13}|^2 = \left|\frac{1}{a_{11}+a_{13}}\right|^2 \\ R_{11} = |r_{11}|^2 = \left|\frac{a_{35}+a_{23}}{a_{11}+a_{13}}\right|^2 \\ T_{21} = |t_{21}|^2 = \left|\frac{1}{a_{35}+a_{37}}\right|^2 \\ T_{23} = |t_{23}|^2 = \left|\frac{1}{a_{35}+a_{37}}\right|^2 \\ R_{11} = |r_{22}|^2 = \left|\frac{a_{45}+a_{47}}{a_{35}+a_{37}}\right|^2 \end{cases} \tag{9}$$

2.2. Analysis of Transmission and Reflection Rates in an Electromagnetic Switch with a Resonator on Each Input Channel

In this section, we calculate the transfer matrix for a Y-shaped electromagnetic switch with a resonator on each input line (Fig. 1(b)). The expressions for the electric fields are presented in

$$E(x,y) = \begin{cases} E_{11}(x) = A_{11}e^{j\alpha_0 x} + B_{11}e^{-j\alpha_0 x} \\ E_{12}(x) = A_{12}e^{j\alpha_1 x} + B_{11}e^{-j\alpha_1 x} \\ E_{13}(y) = A_{13}e^{j\alpha_2 y} + B_{13}e^{-j\alpha_2 y} \\ E_{14}(x) = A_{14}e^{j\alpha_3 x} + B_{14}e^{-j\alpha_3 x} \\ E_{15}(x) = A_{15}e^{j\alpha_4 x} + B_{15}e^{-j\alpha_4 x} \\ E_{16}(y) = A_{16}e^{j\alpha_5 y} + B_{16}e^{-j\alpha_5 y} \\ E_{17}(x) = A_{17}e^{j\alpha_6 x} + B_{17}e^{-j\alpha_6 x} \\ E_{18}(x) = A_{18}e^{j\alpha_7 x} + B_{18}e^{-j\alpha_7 x} \\ E_{19}(x) = A_{19}e^{j\alpha_8 x} + B_{19}e^{-j\alpha_8 x} \\ E_{21}(x) = A_{21}e^{j\alpha_7 x} + B_{21}e^{-j\alpha_7 x} \\ E_{22}(x) = A_{22}e^{j\alpha_6 x} + B_{22}e^{-j\alpha_6 x} \\ E_{23}(y) = A_{23}e^{j\alpha_5 y} + B_{23}e^{-j\alpha_5 y} \\ E_{24}(x) = A_{24}e^{j\alpha_4 x} + B_{24}e^{-j\alpha_4 x} \\ E_{25}(x) = A_{25}e^{j\alpha_3 x} + B_{35}e^{-j\alpha_3 x} \\ E_{26}(y) = A_{26}e^{j\alpha_2 y} + B_{26}e^{-j\alpha_2 y} \\ E_{27}(x) = A_{27}e^{j\alpha_1 x} + B_{27}e^{-j\alpha_1 x} \\ E_{28}(x) = A_{28}e^{j\alpha_0 x} + B_{28}e^{-j\alpha_0 x} \end{cases} \tag{10}$$

Within each medium, the electric field is expressed as the sum of an incident wave and a reflected wave. The amplitudes A_{1i}, B_{1i}, A_{2i}, B_{2i} (for $i = 1, 8$) represent the amplitudes of the

progressive and regressive electromagnetic waves. The propagation constant α_i is defined as:

$$\alpha_i = \frac{\omega}{c}\sqrt{\varepsilon_i \mu_i} \quad \text{for } i = 0, ..., 8 \tag{11}$$

where:

- ω is the angular frequency of the incoming electromagnetic wave
- ε_i is the relative permittivity
- μ_i is the permeability of the non-magnetic medium
- c is the speed of electromagnetic waves in a vacuum

For our calculations, we assume a dielectric permittivity of ($\varepsilon = 2.3$) (polyethylene) and a non-magnetic medium permeability of ($\mu = 1$). These parameters are applied to the segments and resonators that constitute the electromagnetic switch.

To calculate the transfer matrix of our system, we will first determinate the transfer matrix from the first input line to output line. Next, we calculate the transfer matrix from the second input line to output line. This approach allows us to analyze each input channel independently, then combine them to obtain a complete global understanding of the system's behavior.

The transfer matrix for a segment T_{G_x} is defined as:

$$T_{G_x} = \begin{pmatrix} \cos(\alpha d_x) & \frac{-j\sin(\alpha d_x)}{\alpha} \\ -j\alpha \sin(\alpha d_x) & \cos(\alpha d_x) \end{pmatrix} \tag{12}$$

where:

- $\alpha = \frac{\omega}{c}\sqrt{\varepsilon\mu}$ is the propagation constant
- d_x is the length of the segment
- $j = \sqrt{-1}$ is the imaginary unit

For a combination of a segment and a resonator, the transfer matrix $T_{G_x R_y}$ is given by:

$$T_{G_x R_y} = \begin{pmatrix} \cos(\alpha d_x) + \sin(\alpha d_x)\tan(\alpha d_y) & \frac{-j\sin(\alpha d_x)}{\alpha} \\ -j\alpha\sin(\alpha d_x) + j\alpha\cos(\alpha d_x)\tan(\alpha d_y) & \cos(\alpha d_x) \end{pmatrix} \tag{13}$$

where d_y is the height of the resonator.

The derivation of the transfert matrix elements in Eq. (13) wa provided by Touiss et al. [25].

To calculate the transfer matrix from the first input line to the output line, which relates the first input amplitudes to the output amplitudes, we proceed as follows:

Initially, the transfer matrix $T_{G_0 R_1} T_{G_0}$ relates the amplitudes A_{14} and B_{14} to A_{11} and B_{11}:

$$\begin{pmatrix} A_{11} \\ B_{11} \end{pmatrix} = T_{G_0 R_1} T_{G_0} \begin{pmatrix} A_{14} \\ B_{14} \end{pmatrix}$$

Subsequently, the amplitudes A_{14} and B_{14} are connected to A_{15}, B_{15}, A_{19}, and B_{19} using the transfer matrix derived for the electromagnetic switch without resonators. This transfer matrix effectively links the input amplitudes of the first line to output amplitudes:

$$\begin{pmatrix} A_{14} \\ B_{14} \end{pmatrix} = \begin{pmatrix} G_{11} & G_{12} & G_{13} & G_{14} \\ G_{15} & G_{16} & G_{17} & G_{18} \end{pmatrix} \begin{pmatrix} A_{15} \\ B_{15} \\ A_{19} \\ B_{19} \end{pmatrix}$$

The amplitudes A_{15} and B_{15} are related to the output amplitudes A_{18} and B_{18} via the transfer matrix $T_{G_2 R_3} T_{G_2}$:

$$\begin{pmatrix} A_{15} \\ B_{15} \end{pmatrix} = T_{G_2 R_3} T_{G_2} \begin{pmatrix} A_{18} \\ B_{18} \end{pmatrix}$$

By substituting the expression of $\begin{pmatrix} A_{15} \\ B_{15} \end{pmatrix}$ into the transfer matrix, we obtain:

$$\begin{pmatrix} A_{14} \\ B_{14} \end{pmatrix} = \begin{pmatrix} G_{11} & G_{12} \\ G_{15} & G_{16} \end{pmatrix} T_{G_2 R_3} T_{G_2} \begin{pmatrix} A_{18} \\ B_{18} \end{pmatrix} + \begin{pmatrix} G_{13} & G_{14} \\ G_{17} & G_{18} \end{pmatrix} \begin{pmatrix} A_{19} \\ B_{19} \end{pmatrix}$$

Similarly, substituting the expression just obtained for $\left(\frac{A_{14}}{B_{14}}\right)$ back into the initial transfer equation $\left(\frac{A_{11}}{B_{11}}\right) = T_{G_0 R_1} T_{G_0} \left(\frac{A_{14}}{B_{14}}\right)$:

$$\begin{pmatrix} A_{11} \\ B_{11} \end{pmatrix} = T_{G_0 R_1} T_{G_0} \left[\begin{pmatrix} G_{11} & G_{12} \\ G_{15} & G_{16} \end{pmatrix} T_{G_2 R_3} T_{G_2} \begin{pmatrix} A_{18} \\ B_{18} \end{pmatrix} + \begin{pmatrix} G_{13} & G_{14} \\ G_{17} & G_{18} \end{pmatrix} \begin{pmatrix} A_{19} \\ B_{19} \end{pmatrix} \right]$$

Through matrix multiplication, the overall transfer matrix connecting the input amplitudes A_{11} and B_{11} from the first input line to the output amplitudes A_{18}, B_{18}, A_{19}, and B_{19} is obtained as:

$$\begin{pmatrix} A_{11} \\ B_{11} \end{pmatrix} = \begin{pmatrix} H_{11} & H_{12} & H_{13} & H_{14} \\ H_{15} & H_{16} & H_{17} & H_{18} \end{pmatrix} \begin{pmatrix} A_{18} \\ B_{18} \\ A_{19} \\ B_{19} \end{pmatrix} \tag{14}$$

Here, the matrix $T_3 = \begin{pmatrix} H_{11} & H_{12} & H_{13} & H_{14} \\ H_{15} & H_{16} & H_{17} & H_{18} \end{pmatrix}$ represents the elements of the transfer matrix that connect the input amplitudes from the first input line to the output amplitudes in our electromagnetic switching system, which includes a resonator on each input line.

To calculate the transfer matrix from the second input line to the output line, which relates the second input amplitudes to the output amplitudes, we proceed as follows:

Initially, the transfer matrix $T_{G_2 R_3} T_{G_2}$ relates the amplitudes A_{24} and B_{24} to A_{21} and B_{21}:

$$\begin{pmatrix} A_{21} \\ B_{21} \end{pmatrix} = T_{G_2 R_3} T_{G_2} \begin{pmatrix} A_{24} \\ B_{24} \end{pmatrix}$$

Subsequently, the amplitudes A_{24} and B_{24} are connected to A_{25}, B_{25}, A_{29}, and B_{29} using the transfer matrix derived for the electromagnetic switch without resonators. This transfer matrix effectively links the input amplitudes of the second line to the output amplitudes:

$$\begin{pmatrix} A_{24} \\ B_{24} \end{pmatrix} = \begin{pmatrix} G_{21} & G_{22} & G_{23} & G_{24} \\ G_{25} & G_{26} & G_{27} & G_{28} \end{pmatrix} \begin{pmatrix} A_{25} \\ B_{25} \\ A_{29} \\ B_{29} \end{pmatrix}$$

The amplitudes A_{25} and B_{25} are related to the output amplitudes A_{28} and B_{28} via the transfer matrix $T_{G_0R_1}T_{G_0}$:

$$\begin{pmatrix} A_{25} \\ B_{25} \end{pmatrix} = T_{G_0R_1}T_{G_0} \begin{pmatrix} A_{28} \\ B_{28} \end{pmatrix}$$

By substituting the expression of $\begin{pmatrix} A_{25} \\ B_{25} \end{pmatrix}$ into the transfer matrix equation, we obtain:

$$\begin{pmatrix} A_{25} \\ B_{25} \end{pmatrix} = \begin{pmatrix} G_{21} & G_{22} \\ G_{25} & G_{26} \end{pmatrix} T_{G_0R_1}T_{G_0} \begin{pmatrix} A_{28} \\ B_{28} \end{pmatrix} + \begin{pmatrix} G_{23} & G_{24} \\ G_{27} & G_{28} \end{pmatrix} \begin{pmatrix} A_{29} \\ B_{29} \end{pmatrix}$$

Similarly, substituting the expression for $\left(\frac{A_{24}}{B_{24}}\right)$ back into the initial transfer equation, $\left(\frac{A_{21}}{B_{21}}\right) = T_{G_2R_3}T_{G_2}\left(\frac{A_{24}}{B_{24}}\right)$:

$$\begin{pmatrix} A_{21} \\ B_{21} \end{pmatrix} = T_{G_2R_3}T_{G_2}\left[\begin{pmatrix} G_{21} & G_{22} \\ G_{25} & G_{26} \end{pmatrix} T_{G_0R_1}T_{G_0} \begin{pmatrix} A_{28} \\ B_{28} \end{pmatrix} + \begin{pmatrix} G_{23} & G_{24} \\ G_{27} & G_{28} \end{pmatrix} \begin{pmatrix} A_{29} \\ B_{29} \end{pmatrix}\right]$$

Through matrix multiplication, the overall transfer matrix connecting the input amplitudes A_{21} and B_{21} from the second input line to the output amplitudes A_{28}, B_{28}, A_{29}, and B_{29} is obtained as:

$$\begin{pmatrix} A_{21} \\ B_{21} \end{pmatrix} = \begin{pmatrix} H_{21} & H_{22} & H_{23} & H_{24} \\ H_{25} & H_{26} & H_{27} & H_{28} \end{pmatrix} \begin{pmatrix} A_{28} \\ B_{28} \\ A_{29} \\ B_{29} \end{pmatrix} \quad (15)$$

Here, the matrix $T_4 = \begin{pmatrix} H_{11} & H_{12} & H_{13} & H_{14} \\ H_{15} & H_{16} & H_{17} & H_{18} \end{pmatrix}$ represents the elements of the transfer matrix that connect the input amplitudes from the second input line to the output amplitudes in our electromagnetic switching system, which includes a resonator on each input line.

Using the matrices T_3 and T_4, we obtain the following form of the global matrix for our proposed system with a resonator on each input line:

$$\begin{pmatrix} A_{11} \\ B_{11} \\ A_{21} \\ B_{21} \end{pmatrix} = T_{S_2} \begin{pmatrix} A_{18} \\ B_{18} \\ A_{19} \\ B_{19} \\ A_{28} \\ B_{28} \\ A_{29} \\ B_{29} \end{pmatrix} \quad (16)$$

where $T_{S_2} = \begin{pmatrix} b_{11} & b_{12} & b_{13} & b_{14} & b_{15} & b_{16} & b_{17} & b_{18} \\ b_{21} & b_{22} & b_{23} & b_{24} & b_{25} & b_{26} & b_{27} & b_{28} \\ b_{31} & b_{32} & b_{33} & b_{34} & b_{35} & b_{36} & b_{37} & b_{38} \\ b_{41} & b_{42} & b_{43} & b_{44} & b_{45} & b_{46} & b_{47} & b_{48} \end{pmatrix}$.

The transmission and reflection coefficients are represented by the following formulas:

$$\begin{cases} t_{12} = \frac{A_{18}}{A_{11}}\Big)_{B_{18}=0,\ B_{19}=0,\ B_{28}=0,\ B_{29}=0} \\ t_{13} = \frac{A_{19}}{A_{11}}\Big)_{B_{18}=0,\ B_{19}=0,\ B_{28}=0,\ B_{29}=0} \\ r_{11} = \frac{B_{11}}{A_{11}}\Big)_{B_{18}=0,\ B_{19}=0,\ B_{28}=0,\ B_{29}=0} \\ t_{21} = \frac{A_{28}}{A_{21}}\Big)_{B_{18}=0,\ B_{19}=0,\ B_{28}=0,\ B_{29}=0} \\ t_{23} = \frac{A_{29}}{A_{21}}\Big)_{B_{18}=0,\ B_{19}=0,\ B_{28}=0,\ B_{29}=0} \\ r_{22} = \frac{B_{21}}{A_{21}}\Big)_{B_{18}=0,\ B_{19}=0,\ B_{28}=0,\ B_{29}=0} \end{cases} \quad (17)$$

where:

- t_{12}: transmission from input channel 1 through input channel 2.
- t_{13}: transmission from input channel 1 through output channel.
- r_{11}: reflection from input channel 1.

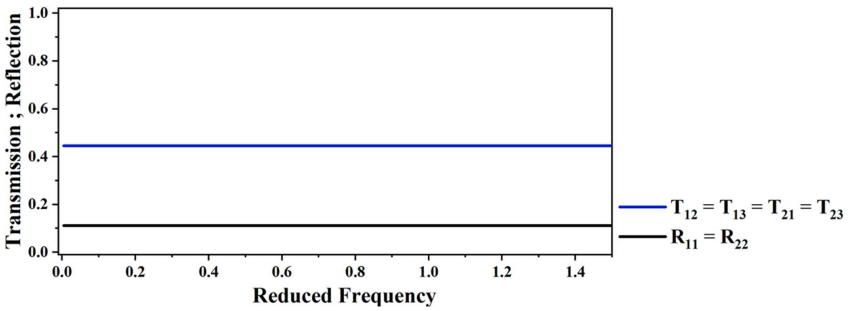

FIGURE 2. Variation of the transmission and reflection rates of the electromagnetic switch system as function of reduced frequency [27].

- t_{21}: transmission from input channel 2 through input channel 1.
- t_{23}: transmission from input channel 2 through output channel.
- r_{22}: reflection from input channel 2.

The transmission and reflection rates are expressed as follows:

$$\begin{cases} T_{12} = |t_{12}|^2 \\ T_{13} = |t_{13}|^2 \\ R_{11} = |r_{11}|^2 \\ T_{21} = |t_{21}|^2 \\ T_{23} = |t_{23}|^2 \\ R_{11} = |r_{22}|^2 \end{cases} \tag{18}$$

3. RESULTS AND DISCUSSIONS

In this study, we examine an electromagnetic switch with two input lines made of waveguides, and each is grafted by a resonator of lengths d_1 and d_3, respectively, and one output channel that consists of semi-infinite segment (Fig. 1(b)). We use a relative dielectric permittivity $\varepsilon = 2.3$ (polyethylene) and a relative magnetic permeability $\mu = 1$ for the segments and resonators. In our calculations, we set the segment length as $d_0 = 1D$. The boundary condition at the ends of the resonators is $E = 0$, and the reduced frequency is $\Omega = \frac{\omega\sqrt{\varepsilon\mu}}{c}D$, where c is the speed of electromagnetic waves in a vacuum, and ω represents the angular pulsation (s^{-1}). We focus on frequencies in the MHz range for characteristic lengths in the meter range, and such a condition corresponds to very low attenuation; therefore, we neglect the imaginary part of dielectric permittivity.

3.1. Analysis of the Electromagnetic Switch System without Resonator

In this part, our objective is to analyze the transmission spectra: T_{12} from input channel 1 to output channel 2 (blue), T_{13} from input channel 1 to output channel (blue), T_{21} from input channel 2 to output channel 1 (blue), and T_{23} from input channel 2 to output channel (blue), as shown in Figure 2. Also, we analyze the reflection spectra: R_{11} in input channel 1 (black) and R_{22} in input channel 2 (black) of a Y-shaped electromagnetic switch system without a resonator as functions of the reduced frequency Ω. In Fig. 2, we show that the transmission rates T_{12}, T_{21}, T_{13}, and T_{23} are steady at around 0.44 while the reflection rates R_{11} and R_{22} are about 0.11 showing that these rates are constant over the range of reduced frequencies $\Omega = [0–1.5]$. It indicates that the system is not efficiently directing the input electromagnetic wave to the single output, demonstrating the limitations of the switch without a resonator. Therefore, it is essential to add resonators to allow better control of electromagnetic wave propagation and improve switch performance by efficiently guiding the signal to the output. Similar results were found by El-Atmani et al. in their study of an acoustic switch, where they concluded that the addition of a resonator was essential to improving switch efficiency [21]. Moreover, in our recent work, we demonstrated that switches without resonators insufficiently controled electromagnetic waves [27]. Introducing a resonator in input 1 transmits waves from input 2 to the output, but only for waves launched from input 2. In the present study, we place a resonator in each input line. The resonators in each input line allow electromagnetic waves from input 1 to reach the output while simultaneously blocking electromagnetic waves from input 2 at the output.

3.2. The Effect of Resonator Heights d_1 and d_2 on Switch System Electromagnetic Wave

In this section, it is essential to understand the role of resonator heights d_1 and d_3 in controlling and directing electromagnetic waves in an electromagnetic switch system. Fig. 3 shows the transmission spectra: T_{13} from input channel 1 to output channel (red), T_{12} from input channel 1 to input channel 2 (green), T_{21} from input channel 2 to input channel 1 (orange), and T_{23} from input channel 2 to output channel (blue). It also examines the reflection spectra: R_{11} in input channel 1 (purple) and R_{22} in input channel 2 (black) as functions of the reduced frequency Ω for $d_0 = d_2 = 2.0D$. The segment lengths d_0 and d_2 are kept constant while the resonator heights d_1 and d_3 are varied. The aim is to determine how adjusting the resonator lengths d_1 and d_3 to find matching conditions can direct electromagnetic waves, allowing passage from input 1 to the output ($T_{13} = 1$) while blocking waves from input 2 ($T_{23} = 0$) or vice versa ($T_{23} = 1, T_{13} = 0$).

In Fig. 3(a), with $d_1 = 1.85D$ and $d_3 = 0.15D$, the transmission spectrum $T_{13} = 0.97$ is observed within the frequency range $\Omega = [0.66; 0.82]$, while the transmission $T_{23} = 0.01$ is minimized within the same range. This indicates that the system effectively transmits almost all electromagnetic waves

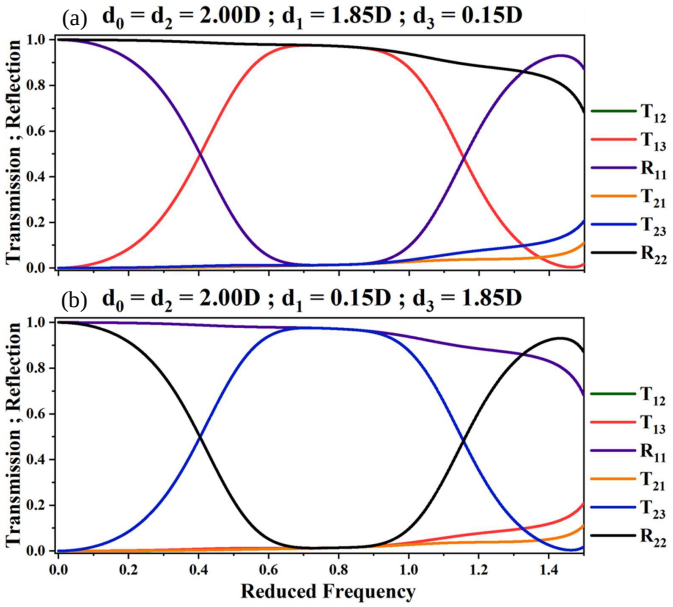

FIGURE 3. Variation of the transmission and reflection rates T_{12}, T_{13}, T_{21}, T_{23}, R_{11} and R_{22} of the electromagnetic switch as function of reduced frequency with $d_0 = d_2 = 2D$, for different values of the heights resonator d_1 and d_3: (a) $d_1 = 1.85D$ and $d_3 = 0.15D$; (b) $d_1 = 0.15D$ and $d_3 = 1.85D$.

from input 1 to the output (ON state) while blocking waves from input 2 to the output (OFF state). These results demonstrate the effectiveness of utilizing a taller resonator height d_1 and a shorter resonator height d_3 to achieve a precise switching behavior from the first input to the output channel. Conversely, in Fig. 3(b), with $d_1 = 0.15D$ and $d_3 = 1.85D$, the transmission spectrum changes, $T_{23} = 0.97$ within the frequency range $\Omega = [0.66; 0.82]$, while the transmission $T_{13} = 0.01$ is minimized. This configuration indicates that the switch is ON for the transmission of electromagnetic waves from input 2 to output channel, while blocking waves from input 1 to output. These results show the essential role of precise adjustments to resonator heights d_1 and d_3 in the control of ON and OFF states, allowing efficient routing of electromagnetic waves in the switching system. The study concludes that for $T_{13} = 1$ and $T_{23} = 0$, the condition $d_1 \gg d_3$ must be satisfied, while for $T_{13} = 0$ and $T_{23} = 1$, $d_1 \ll d_3$ is necessary. The generalized conditions are expressed as: $d_1 = 1D + \delta$ and $d_3 = 1D - \delta$, where $-1 < \delta < 1$. This provides a simplified expression to study the effect of resonator height for optimal wave electromagnetic transmission control.

3.3. Adjustments of Resonator Height to Control the Electromagnetic Waves

In this part, we examine the variation of the resonator heights d_1 and d_3 by applying the conditions $d_1 = 1D + \delta$ and $d_3 = 1D - \delta$. Our aim is to achieve efficient switching between two states: $T_{13} = 1$ and $T_{23} = 0$ (where electromagnetic waves from input 1 are transmitted to the output (ON), while waves from input 2 are blocked from the output (OFF))), or $T_{13} = 0$ and $T_{23} = 1$ (where waves from input 1 are blocked from the output (OFF), and waves from input 2 are transmitted to the output (ON)). These states are achieved by adjusting δ to control the switching behavior. Fig. 4 presents the transmission spectra: T_{13}, T_{12}, T_{21}, T_{23} as well as the reflection spectra: R_{11} and R_{22} as functions of the reduced frequency Ω with $d_0 = d_2 = 2.0D$. The segment lengths d_0 and d_2 are kept constant while the resonator heights d_1 and d_3 are varied by δ.

In Fig. 4(a) with $\delta = 0.98D$, transmission through the output line $T_{13} = 1$ in the frequency range $\Omega = [0.66; 0.82]$ demonstrates efficient switching, allowing complete transmission of electromagnetic waves from input 1 to the output (ON). At the same time, $T_{23} = 0$ in the same frequency range confirms complete blocking of electromagnetic waves from input 2 to the output (OFF). Zero reflection $R_{11} = 0$, indicates that the system switches and efficiently directs electromagnetic waves from input 1 without significant losses. These states are obtained by ensuring $d_1 \gg d_3$. In Fig. 4(b) with $\delta = 0.86D$, $T_{13} = 0.97$ within the frequency range $\Omega = [0.65; 0.85]$ indicates efficient switching, allowing nearly full transmission of electromagnetic waves from input 1 to the output. At the same time, $T_{23} = 0.02$ almost completely blocks electromagnetic wave transmission from input 2 to the output. In Fig. 4(c), with $\delta = 0.6D$, $T_{13} = 0.8$ and $T_{23} = 0.08$ show a partial distribution of electromagnetic energy at the output, with no clear ON/OFF state. The system is not very effective at switching, as the electromagnetic waves are not completely blocked or fully transmitted from input line 1 or 2 to the output line. In contrast, in Fig. 4(d), with $\delta = 0D$, $T_{13} = T_{23} = 0.66$, the transmission of electromagnetic waves is distributed uniformly across the output line, without clear ON/OFF states. This indicates that there is ineffective switching behavior in the system as electromagnetic waves are transmitted equally from input 1 and input 2 to the output, making it impossible to control the direction of electromagnetic wave transmission. In Fig. 4(e), with $\delta = -0.86D$, $T_{23} = 0.97$ in the range frequency $\Omega = [0.65; 0.85]$ indicates efficient switching, allowing nearly full transmission of electromagnetic waves from input 2 to output (ON), while $T_{13} = 0.02$ reflects nearly complete blocking from input line 1 to output line. In Fig. 4(f), with a more negative $\delta = -0.98D$, the system shows its ability to fully reverse the electromagnetic wave transmission, enabling complete transmission from input line 2 to the output channel and total blocking from input line 1 to output line. The combined influence of d_1 and d_3 shows that adjusting the two resonator heights with δ allows precise control of the direction of electromagnetic waves. With a positive δ, ensuring $d_1 \gg d_3$, electromagnetic waves are transmitted from input 1 to output (ON), while blocking waves from input 2 (OFF). Conversely, with a negative δ, ensuring $d_1 \ll d_3$, the behavior is reversed. By precisely adjusting these parameters, we can efficiently control the direction of electromagnetic waves and achieve precise ON/OFF switching.

3.4. Directional Control of Electromagnetic Waves: The Parameter δ Effect

Figure 5 illustrates that the reduced frequency of resonant modes varies with the parameter δ. The red branches represent the maximum transmission T_{13}, while the blue branches indicate the maximum transmission T_{23}. As δ increases positively,

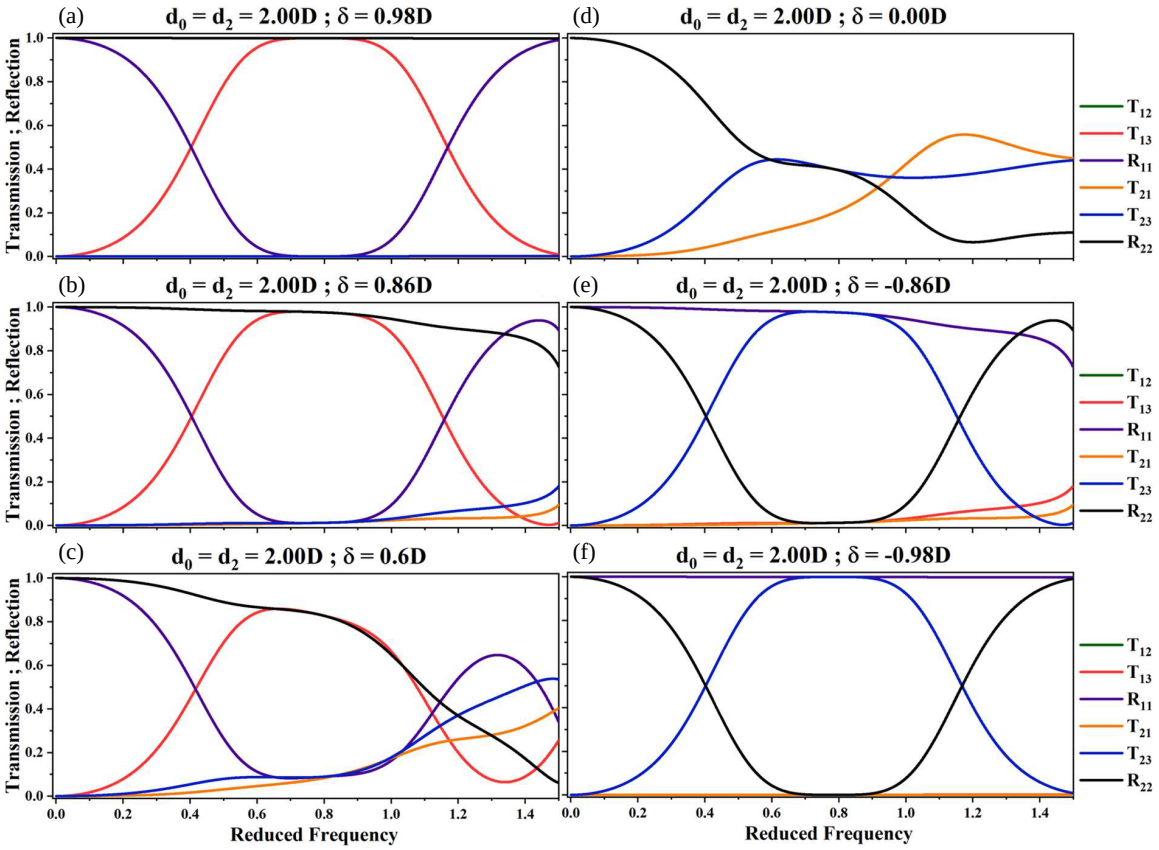

FIGURE 4. Variation of the transmission and reflection rates T_{12}, T_{13}, T_{21}, T_{23}, R_{11} and R_{22} of the electromagnetic switch as function of reduced frequency, for different values of δ: (a) $\delta = 0.98D$; (b) $\delta = 0.86D$; (c) $\delta = 0.6D$; (d) $\delta = 0.0D$; (e) $\delta = -0.86D$; and (f) $\delta = -0.98D$.

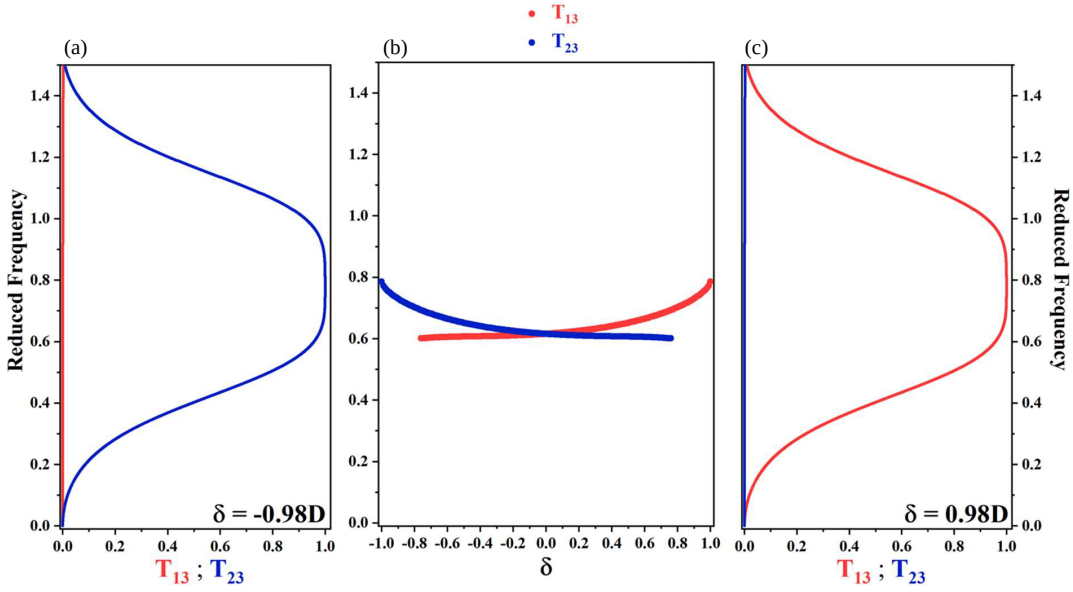

FIGURE 5. Variation of the reduced frequency as a function of the transmission rates T_{13} (red color), T_{23} (blue color) through the output line for: (a) $\delta = -0.98D$ and (c) $\delta = 0.98D$. (b) Variation of the reduced frequency as function parameter δ.

T_{13} approaches 1 within specific frequency ranges, demonstrating efficient transmission from input 1 to the output line (ON), while T_{23} approaches 0, effectively blocking input 2 to output line (OFF). Conversely, when δ takes on negative values, T_{23} nears 1, and T_{13} approaches 0, reversing the transmission direction. For intermediate values of δ ($\delta = 0$), two rates demonstrate a mixed transmission response, which reduces the clarity of the switching mechanism. This tunability of the coefficients

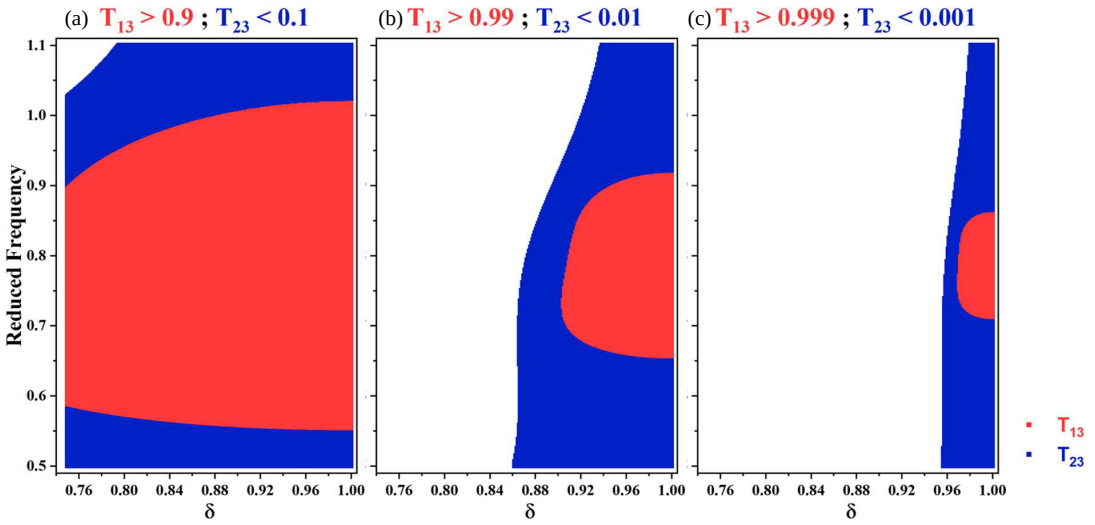

FIGURE 6. Electromagnetic switching efficiency: variation of maximum T_{13} and minimum T_{23} transmission rates as function parameter δ for (a) $T_{13} > 0.9$, (b) $T_{13} > 0.99$, and (c) $T_{13} > 0.999$.

enables precise control over the direction of electromagnetic waves, facilitating reliable ON/OFF switching based on the selected coefficient value for effective electromagnetic control in our system.

3.5. Electromagnetic Switches with Parameter Positive δ for Maximum T_{13} and Minimum T_{23} Transmission Rates

In this study, we examine the operation of an electromagnetic switch that alternates between ON and OFF states (Fig. 6). This figure shows the maximum transmission T_{13} and the minimum T_{23}, giving important information about the switch's performance at different frequencies. We take the value of δ positive to obtain the case allowing to transmit electromagnetic waves to pass from input 1 to the output (T_{13}) in the state ON, while in the OFF state, it effectively blocks the waves from input 2 to the output (T_{23}), resulting in minimal or no transmission. The figure represents the different maximum transmission values of T_{13} (red area) and different minimum transmission values of T_{23} (blue area) providing insights into the system's switching behavior across various frequencies. Based on the analysis of these curves, the parameter δ is changed to maximize the functionality of the switch. We use specific transmission thresholds: $T_{13} > 0.9$, $T_{13} > 0.99$, $T_{13} > 0.999$ for T_{13}, and $T_{23} < 0.1$, $T_{23} < 0.01$, and $T_{23} < 0.001$ for T_{23}, to characterize the system's switching capabilities. In the first case (Fig. 6(a)), the red area indicates that the transmission reaches a maximum of 90% around $\delta = 1$, in the frequency range [0.4–1.1]. In the second case (Fig. 6(b)), the red area shows that the transmission reaches a maximum of 99% around $\delta = 1$, in the frequency range [0.5–0.91]. Finally, in the third case (Fig. 6(c)), the red area indicates that the transmission reaches a maximum of 99.9% around $\delta = 1$, in the frequency range [0.7–0.85]. These results demonstrate how increasing the switching rate affects performance within the same frequency range. Moreover, adjusting the resonator heights helps optimize the switching rate in specific frequency intervals. This shows that the switch rate is a crucial performance indicator, reflecting the system's ability to meet the required transmission thresholds in the output lines. Similar findings were reported by El-Atmani et al. in their study of an acoustic switch, where they observed comparable results [26].

3.6. Electromagnetic Switch Efficiency with Negative Parameter δ for Maximum T_{23} and Minimum T_{13} Transmission Rates

In this study, we examine the reduced frequency as a function of the negative value of δ (Fig. 7), facilitating the understanding of the system's behavior. In this inverse case, compared to the situation shown in Fig. 6 where δ is positive, the system allows electromagnetic waves to pass from input 2 to the output (T_{23}) in the ON state, while blocking the waves from input 1 to the output (T_{13}) in the OFF state. The figure displays maximum transmission values of T_{23} (blue area) and minimum values of T_{13} (red area), providing insights into the system's switching behavior. Transmission thresholds are used to characterize performance, with $T_{23} > 0.9$, $T_{23} > 0.99$, $T_{23} > 0.999$ for T_{23}, and $T_{13} < 0.1$, $T_{13} < 0.01$, and $T_{13} < 0.001$ for T_{13}. The analysis demonstrates that adjusting the resonator heights improves switching rate efficiency within specific frequency ranges.

3.7. Analysis of Electromagnetic Switching Behavior Based on Positive and Negative δ

In this section, we analyze the behavior of an electromagnetic switch (ON/OFF) that operates selectively based on the sign of parameter δ. For positive δ, where the condition $d_1 \gg d_3$ realized, the switch allows the transmission T_{13} of electromagnetic waves from input 1 to the output, while simultaneously blocking transmission T_{23} of waves from input 2 to output. Conversely, for negative δ, where $d_1 \ll d_3$, the system permits transmission T_{23} of electromagnetic waves from input 2 to the output and blocks transmission T_{13} of waves from input 1 to

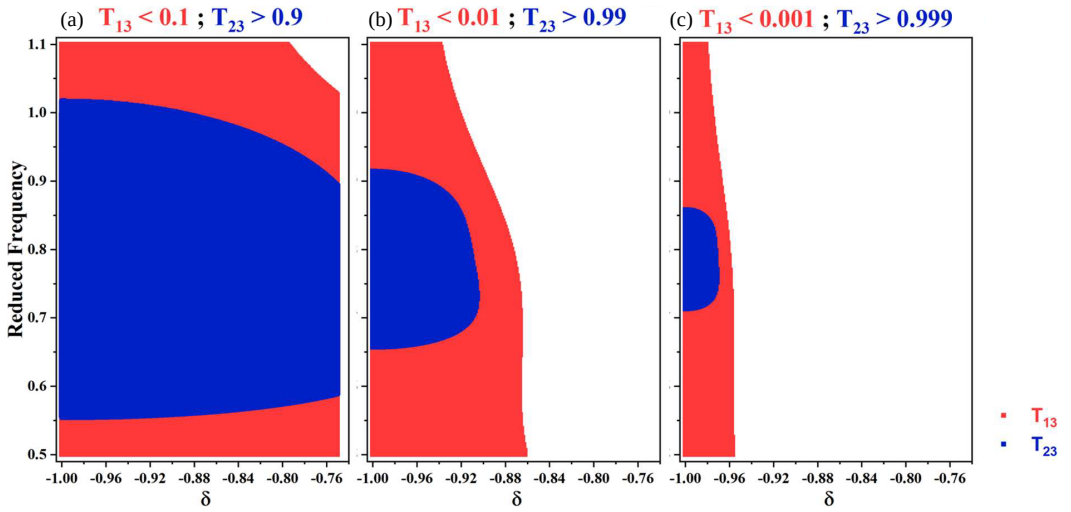

FIGURE 7. Electromagnetic switching efficiency: variation of maximum T_{23} and minimum T_{13} transmission rates as function parameter δ for (a) $T_{23} > 0.9$, (b) $T_{23} > 0.99$, and (c) $T_{23} > 0.999$.

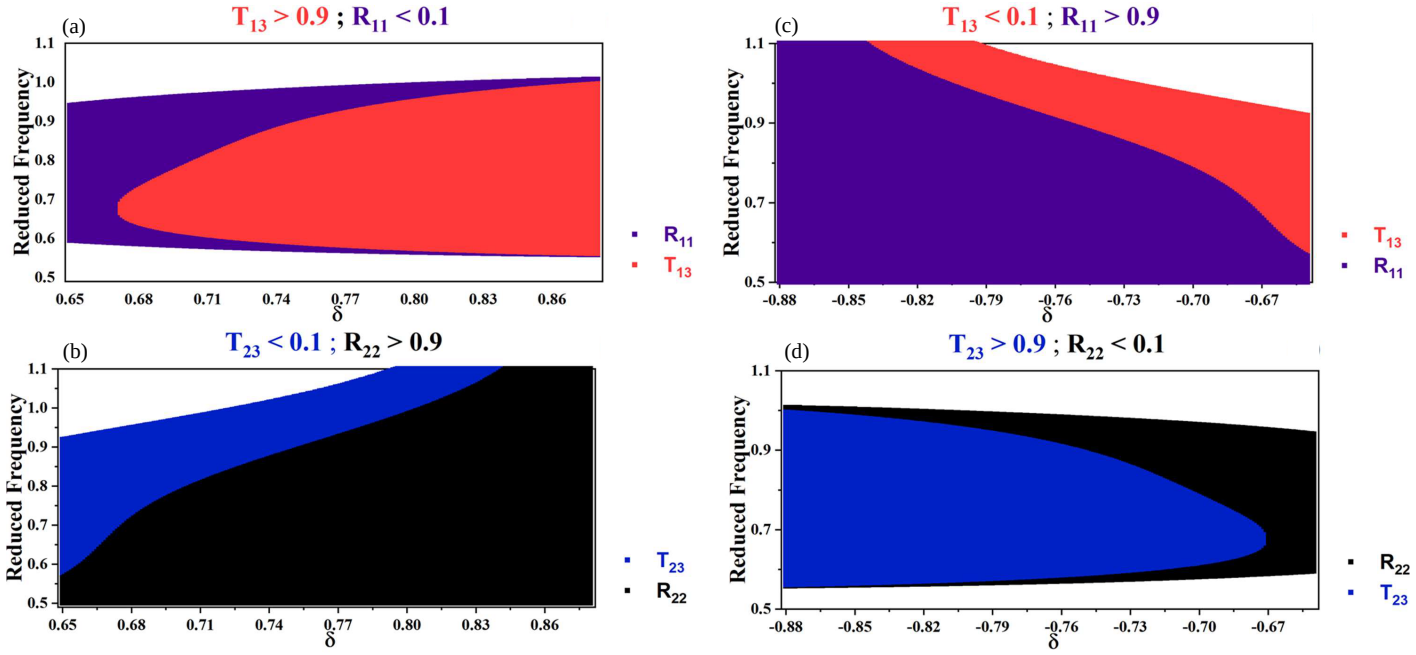

FIGURE 8. Schematic representation and behavioural analysis of electromagnetic switching.

output. The colored area in the figures (Fig. 8) corresponds to specific operational thresholds of the switch. For positive δ, the red area (T_{13}) indicates maximum transmission through output; the blue area (T_{23}) represents minimum transmission through output; the black area (R_{22}) indicates maximum reflection from input 2; and the purple area represents minimum reflection (R_{11}) from input 1. For negative δ, the behavior shifts: the red area indicates minimum transmission (T_{13}) through output; the blue area represents maximum transmission (T_{23}) from input 2 through output; the black area indicates minimum reflection (R_{22}) from input 2, while the purple area highlights maximum reflection (R_{11}) from input 1.

In Fig. 8(a), under the desired thresholds transmission and reflection $T_{13} > 0.9$ and $R_{11} < 0.1$ with positive value of parameter δ, the switch effectively transmits waves from input 1 to output, showing stable behavior in a range of reduced frequency specific. In Fig. 8(b), with $T_{23} < 0.1$ and $R_{22} > 0.1$, the system blocks waves from input 1, confirming strong reflection. For negative value of parameter δ, Fig. 8(c) demonstrates that $T_{13} < 0.1$ and $R_{11} > 0.9$, meaning that the system primarily reflects waves from input 1. In Fig. 8(d), where $T_{23} > 0.9$ and $R_{22} < 0.1$, the system allows efficient transmission from input 2 to output, demonstrating the versatility of the switch. In summary, the system effectively switches between transmission and reflection based on the sign and value of δ, ensuring precise control over wave propagation in both ON and OFF states.

4. CONCLUSION

The purpose of this paper was to present and analyze a Y-shaped electromagnetic waveguide switch that enables the efficient and precise control of electromagnetic wave propagation. Our investigation confirmed that this switch can achieve selective transmission from one input channel to the output while effectively blocking the other input or inverse, depending on the resonator configurations. By using Transfer Matrix Method (TMM), we observed that adjusting the resonator heights and segment lengths within the waveguide structure enabled near-total transmission in the ON state, achieving rates above 99%, while maintaining minimal transmission (below 1%) in the OFF state. These results highlight the critical role of resonator tuning in achieving the desired switching behavior and demonstrate the effectiveness of our design for applications that require high levels of signal precision and control. The study further indicates that the system's performance can be optimized over a wider frequency range by adjusting the resonator characteristics, suggesting that the switch is adaptable for broader spectral applications. This adaptability, combined with the switch's high transmission efficiency, underscores its potential for integration into optical communication systems. Future perspectives include experimental validations to verify theoretical outcomes and adjustments to enhance frequency versatility, making the switch a strong candidate for advanced signal processing and telecommunications applications that demand reliable wave directionality and adaptability.

REFERENCES

[1] Hu, Y., M. Tong, S. Hu, W. He, X. Cheng, and T. Jiang, "Reassessing fano resonance for broadband, high-efficiency, and ultrafast terahertz wave switching," *Advanced Science*, Vol. 10, No. 2, 2204494, 2023.

[2] Hill, M. T., "Optical waveguide switch based on a negative-index metamaterial load," *Optics Letters*, Vol. 48, No. 4, 948–951, 2023.

[3] Zhang, Y., S. Ouyang, Y. Zhang, X. Su, and Q. Kuang, "Design of high isolation waveguide switch component in Ka band for SAR system," in *2022 3rd China International SAR Symposium (CISS)*, 1–4, Shanghai, China, Nov. 2022.

[4] Rehman, A. U., Y. Khan, M. Irfan, and M. A. Butt, "Investigation of optical-switching mechanism using guided mode resonances," *Photonics*, Vol. 10, No. 1, 13, 2023.

[5] MacDonald, R. G., A. Yakovlev, and V. Pacheco-Peña, "Amplitude-controlled electromagnetic pulse switching using waveguide junctions for high-speed computing processes," *Advanced Intelligent Systems*, Vol. 4, No. 12, 2200137, 2022.

[6] Lin, M., Z. Tang, L. Huang, Z. Jiang, and J. Huangfu, "A waveguide filter with switchable pass-band and stop-band," in *2020 9th Asia-Pacific Conference on Antennas and Propagation (APCAP)*, 1–2, Xiamen, China, Aug. 2020.

[7] Agrahari, R., S. K. Ghosh, and S. Bhattacharyya, "Optical switches," in *Optical Switching: Device Technology and Applications in Networks*, 13–30, D. Nandi et al. (eds.), Wiley, 2022.

[8] Yajima, S., N. Nishiyama, and Y. Shoji, "High-speed modulation in a waveguide magneto-optical switch with impedance-matching electrode," *Optics Express*, Vol. 31, No. 10, 16 243–16 250, 2023.

[9] Soref, R., "Tutorial: Integrated-photonic switching structures," *APL Photonics*, Vol. 3, 021101, 2018.

[10] Shen, S. C., C. T. Pan, and H. P. Chou, "Electromagnetic optical switch for optical network communication," *Journal of Magnetism and Magnetic Materials*, Vol. 239, No. 1-3, 610–613, 2002.

[11] Hui, D., H. Alqattan, S. Zhang, V. Pervak, E. Chowdhury, and M. T. Hassan, "Ultrafast optical switching and data encoding on synthesized light fields," *Science Advances*, Vol. 9, No. 8, 2023.

[12] Hui, D., H. Alqattan, S. Zhang, V. Pervak, E. Chowdhury, and M. Hassan, "Attosecond optical switching," 2021, [Online]. Available: https://doi.org/10.21203/rs.3.rs-1232650/v1.

[13] Pochernyaev, V., N. Syvkova, and M. Mahomedova, "Switch-filter on a rectangular waveguide partially filled bydielectric," *Informatyka, Automatyka, Pomiary w Gospodarce i Ochronie Środowiska*, Vol. 12, No. 3, 8–11, 2022.

[14] Bagheriasl, M., J. Sarrazin, and G. Valerio, "Reconfigurable waveguides using glide-symmetric bed of nails: Design of an all-metal switch at millimetre-wave band," 1–8, 2020, [Online]. Available: http://arxiv.org/abs/2007.08021.

[15] Alquliah, A., M. Elkabbash, J. Cheng, G. Verma, C. S. Saraj, W. Li, and C. Guo, "Reconfigurable metasurface-based 1×2 waveguide switch," *Photonics Research*, Vol. 9, No. 10, 2104–2115, 2021.

[16] Jung, H., "An integrated photonic electric-field sensor utilizing a 1×2 YBB Mach-Zehnder interferometric modulator with a titanium-diffused lithium niobate waveguide and a dipole patch antenna," *Crystals*, Vol. 9, No. 9, 459, 2019.

[17] Dao, K. P., J. Hu, and R. Soref, "Design of an ultra-compact, energy-efficient non-volatile photonic switch based on phase change materials," *Journal of Optical Microsystems*, Vol. 4, No. 3, 031204, 2024.

[18] Rehman, A. U., Y. Khan, M. Irfan, S. Choudri, S. N. Khonina, N. L. Kazanskiy, and M. A. Butt, "Three-dimensional modeling of the optical switch based on guided-mode resonances in photonic crystals," *Micromachines*, Vol. 14, No. 6, 1116, 2023.

[19] Rehman, A. U., Y. Khan, M. Irfan, M. A. Butt, S. N. Khonina, and N. L. Kazanskiy, "A novel design of optical switch based on guided mode resonances in dielectric photonic crystal structures," *Photonics*, Vol. 9, No. 8, 580, 2022.

[20] El-Atmani, I., I. E. Kadmiri, A. Khaled, D. Bria, M. E. C. E. Kettani, and P. Marechal, "Three channels splitter acoustic waves based on ramified system made of waveguides and a resonators," in *2024 4th International Conference on Innovative Research in Applied Science, Engineering and Technology (IRASET)*, 1–6, FEZ, Morocco, May 2024.

[21] El-Atmani, I., I. E. Kadmiri, D. Bria, A. Khaled, M. E. C. E. Kettani, and P. Marechal, "Acoustic switch device for a splitter acoustic wave made by waveguides and resonator," in *2024 International Conference on Circuit, Systems and Communication (ICCSC)*, 1–5, Fes, Morocco, Jun. 2024.

[22] Touiss, T., I. E. Kadmiri, Y. Errouas, and D. Bria, "Electromagnetically induced transparency and fano resonances in waveguides and U-shaped or cross-shaped resonators," *Progress In Electromagnetics Research M*, Vol. 127, 53–63, 2024.

[23] Touiss, T., Y. Errouas, A. Ouariach, and D. Bria, "Theoretical design of high-performance guiding and filtering devices using photonic comb-like waveguides with defective resonators," *Journal of Electromagnetic Waves and Applications*, Vol. 38, No. 16, 1779–1795, 2024.

[24] Touiss, T., M. R. Qasem, S. Machichi, F. Falyouni, and D. Bria, "Theoretical study of electromagnetic wave propagation in dielectric cylindrical waveguides," in *2024 International Confer-*

ence on Circuit, Systems and Communication (ICCSC), 1–6, Fes, Morocco, Jun. 2024.

[25] Touiss, T., Y. Errouas, I. E. Kadmiri, and D. Bria, "Electromagnetic filtering with high performance by one dimensional defective comb-like waveguides structure using the transfer matrix," in *The International Conference on Energy and Green Computing (ICEGC'2023)*, Vol. 469, 00091, Fes, Morocco, Nov. 2023.

[26] El-Atmani, I., A. Khaled, D. Bria, M. E. C. E. Kettani, P. Maréchal, *et al.*, "Acoustic splitter waves based on ramified system made of waveguides," in *2024 4th International Conference on Innovative Research in Applied Science, Engineering and Technology (IRASET)*, Vol. 364, 04002, FEZ, Morocco, May 2023.

[27] Chaker, I., Y. Errouas, I. El-atmani, A. Ghadban, D. Bria, and K. Laabidi, "Y-shaped electromagnetic switch using waveguides and a resonator," in *International Conference on Electronic Engineering and Renewable Energy Systems*, 153–163, Saidia, Morocco, 2024.